Study of Inhomogeneity in Large Format Li-Ion Cells with different Multiphysics Models

Sabine Arnold[*1], Raghavendra Arunachala[1], Lemuel Moraleja[1] and Andreas Jossen[1,2]
[1]TUM CREATE Singapore, [2]Institute for Electrical Energy Storage at Technical University of Munich
*Corresponding author: 1 Create Way, #10-02, CREATE Tower, Singapore 138602, sabine.arnold@tum-create.edu.sg

Abstract: Different models are developed with COMSOL Multiphysics to investigate the spatial differences in temperature and current in large format Li-Ion cells. The thermal and electrochemical behaviors of a battery are closely linked. So the models use the COMSOL Lithium-Ion Battery and the Heat Transfer Interface. All are based on the work of Newman et al. [1-3.]. The models are validated by thermal measurement and terminal voltage. Simulation results show considerate inhomogeneity in large format battery cells.

Keywords: Li-Ion, inhomogeneity, coupled electrochemical-thermal model, 3D battery model

1 Introduction

Large format Li-Ion battery pouch cells (LIBC), often employed in electric vehicles (EV), show notable gradients in current and temperature distribution. This inhomogeneity can reduce the utilization of the cell and accelerate battery aging. Additionally, strong inhomogeneity can also influence the cell safety [4]. It is, however, difficult to determine the local temperature and current inside the LIBC experimentally for a detailed analysis.

Multiphysics Finite Element Simulation can help to map and understand their in-cell distribution. Therefore we develop models of different scale and dimensions to investigate a commercially available 63Ah pouch bag LIBC. Galvanostatic discharge experiments allow model validation.

2 Modelling Theory

2.1. Electrochemical Model

The electrochemical processes inside the LIBC can be characterized by porous electrode theory, intercalation reaction kinetics, charge transfer and mass transport in both, solids and concentrated electrolyte. The diffusion of Li- Ion in the active material particles of the electrodes is described by Fick's second law. [1,2]. All equations are listed in Figure 1. The entropic coefficients and the electrolyte transport properties change with the state of charge and are therefore described as a function of the lithium concentration. The latter are also strongly dependent on temperature, as are the reaction rates and the diffusion in the electrodes.

$$j_n = j_0[exp(\frac{n\alpha_a F\eta}{RT}) - exp(-\frac{n\alpha_c F\eta}{RT})]$$ Reaction kinetics

$$j_0 = F(k_a)^{a_c}(k_c)^{a_a}(c_{s,max} - c_s)^{a_a}(c_s)^{a_c}(c)^{a_a}$$ Local current density

$$\eta = \phi_s - \phi_l - U_{OCP}$$ Electrode Potential

$$i_s = I - i_l = -\sigma_{eff}\nabla\phi_s$$

$$\nabla\phi_l = -\frac{j_l}{\kappa} - \frac{2RT}{F}(1-t^+)(1+\frac{d\ln(f)}{d\ln(c)})\nabla lnc$$ Electrolyte Potential

Ion transport in electrolyte

$$\epsilon\frac{\delta c}{\delta t} = \nabla\epsilon D_{chem}(1 - \frac{dlnc_0}{dlnc})\nabla c + \frac{t_-\nabla i_l + i_l\nabla t_-}{z_+\upsilon_+ F} - \nabla c\upsilon_0 + aj_-$$

$$\frac{\delta c_s}{\delta t} = \frac{1}{r^2}\frac{\delta}{\delta r}(D_s r^2\frac{\delta c_s}{\delta r})$$ Ion transport in electrodes

Figure 1: Governing Equations for electrochemical model [1, 2]

2.2. Thermal Model

The electrochemical model is coupled with the energy balance for each arbitrary control volume [5]:

$$\rho c_p\frac{\partial T}{\partial t} = -k\Delta T + Q \quad (1)$$

Heat conduction $-k\Delta T$ is assumed to dominate internal heat transport [7]. The heat generation during standard discharge can be split into two terms:

$$Q = Q_{joul} + Q_{rev} \quad (2)$$

The irreversible heat Q_{joul} occurs due to polarization effects and can be calculated by the internal resistance [3]:

$$Q_{joul} = I^2 R_{internal} \quad (3)$$

This is a simplified description, as not all overpotentials are linear and the cell resistance shows temperature and current dependencies.

Arising from entropic effects during the reactions in the active material, the reversible

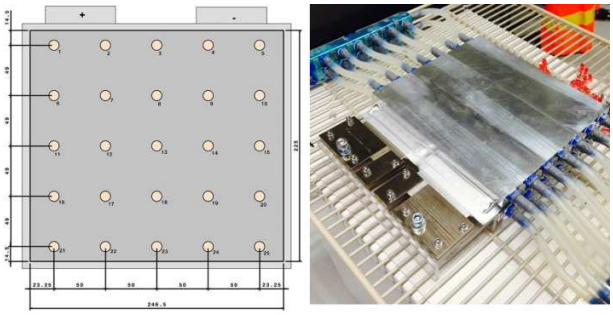

Figure 2: Experiment setup: position of the thermocouples and photo of the cell with sensor matrix for surface temperature measurement and bottom cooling plate

heat Q_{rev} can be described by the simplified impression

$$Q_{rev} = \frac{I}{zF} T\Delta S \qquad (4)$$

Arrhenius correlations describe the temperature dependency of electrochemical properties [6].

3 Experiments for Model Validation

In order to get reliable simulation output we compare voltage and surface temperature data with experiment results.

The modeled and investigated LIBC is a 63Ah high power pouch bag cell with a nominal voltage of 4.2V. The active material consists of a nickel manganese cobalt oxide (NMC) cathode, a graphite anode and a $LiPF_6$ based EC/EMC mixture electrolyte.

The test cell is equipped with a matrix of temperature sensors (thermocouples t-type) (see Figure 2) attached to the top surface and discharged at different C-Rates (1C, 3C, 5C) with a Digatron MCT battery tester at an ambient temperature of 25°C inside a climate chamber (ESPEC PU-3J).

Battery currents are usually indicated in C-Rates, which is a measure of the rate at which a LIBC is discharged relative to its nominal capacity. Thus a 1C rate means the battery will be discharged within 1 hour at this current. For our 63Ah LIBC a 1C discharge current accordingly equates to 63A.

For better control of the surface temperature the experiments are repeated with a water flow controlled aluminum cooling plate at the bottom.

For the validation of single LIBC layer scale models a 1C discharge in an Accelerating Rate Calorimeter (ARC) from Thermal Hazard Technology is performed. The ARC is an adiabatic calorimeter and can simulate quasi adiabatic boundary conditions.

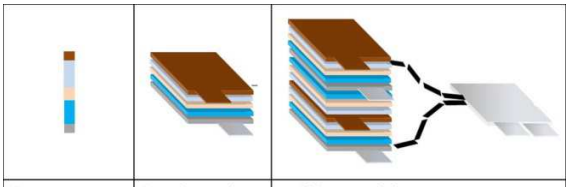

1D Newman	3D electrode sandwich	Full 3D Model (fully coupled and purely thermal)

Table 1: different geometrical model setups

4 COMSOL Models

The mathematical models described in section 2 can be set up with the COMSOL Lithium-Ion Battery and Heat Transfer in Solids interface. Models of different scale and dimensions are set up in order to compare the content value of their simulation results in relation to the computational costs.

4.1. Model Parameters

It is important to adapt the model parameters for large format high power LIBCs. Especially the capacity and geometry of the electrodes can be very different from smaller high energy cells, which can cause convergence problems. For instance, the lithium ion concentration can be reduced dramatically or even reach negative values locally. For real battery systems the local concentration can never be less or equal than zero.

Stewart at al. [9] give a good properties overview for modelling automotive batteries, while Ecker et al. [10] propose a detailed plan to determine the electrochemical parameters of a pouch bag cell with NMC cathode. Valøen and Reimers [11] and Nyman et al. [14] provide a precise analysis of $LiPF_6$ based electrolytes. If not experimentally determined in group, all model parameters are taken from the aforementioned literature (see Appendix 9.1).

4.2. Mesh, component coupling and solver

All models employ user defined meshes with finer meshing at the electrode surfaces to facilitate the computing of the mass transport equations.

2D and 3D model geometries are set up of extremely thin layers. Here a “swept mesh” is more convenient, because the cross-plane mesh elements need to be much finer than the in-plane elements.

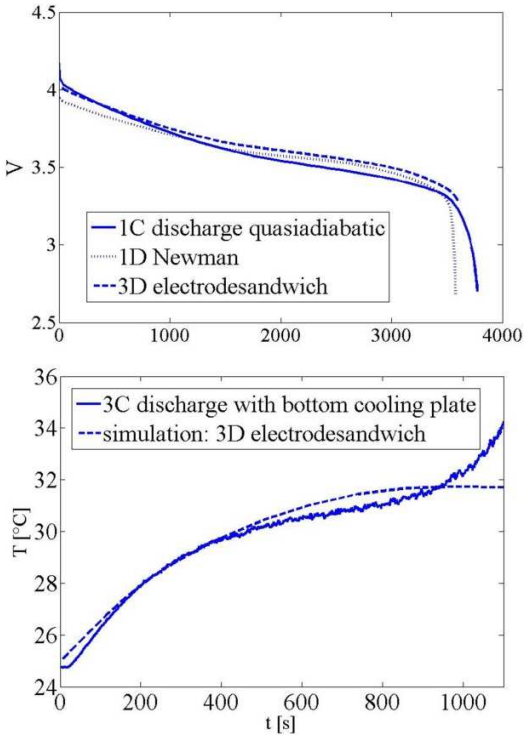

Figure 4: Top: Comparison of the simulated Electrode Potential (isothermal 1D Newman and fully coupled 3D electrode sandwich) and the ARC experiment results for adiabatic 1C discharge, bottom: top surface center temperature development of the full 3D model and the 3C discharge experiment with the bottom cooling plate

As we expect notable gradients in the dependent variables for all domains, we require the COMSOL Identity Mapping operator to couple the thermal and the electrochemical model. The commonly used average operator does not take these spatial differences into account and thus does not provide accurate results.

Due to the highly nonlinear nature of the governing equations the setting of the time dependent solver need to be adjusted. The relative tolerance is set to 1e-4, the dependent variables are scaled manually beforehand and the nonlinear method is switched to Constant (Newton) and set to make a Jacobian Update on every iteration.

4.3. 1D Newman

To reduce complexity and computing time we use a simple isothermal 1D model (see Table 1), commonly referred to as the classic Newman model [5], for parametrization and validation of

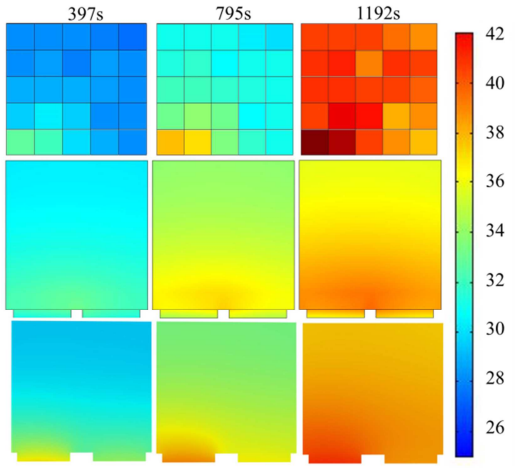

Figure 3: Top surface temperature distribution during 3C discharge, top: thermocouple measurements, middle: fully coupled 3D simulation, bottom: 3D thermal only simulation

the electrochemical model. As for all single layer scale models the input current density needs to be adapted. The cell layers are stacked in parallel. So the current needs to be divided by the number of cathodes.

4.4. 3D single layer

To include thermal effects and to learn about the spatial distribution of the dependent variables, the next step is a fully coupled 3D model of a single LIBC layer, or electrode sandwich (3D ES) (see Table 1). The electrochemical model is formed of the negative current collector, the anode, the separator, the cathode and the positive current collector. For the thermal model averaged material properties are assumed for all domains.

For low discharge rate and regular operation, heat will be released relatively slowly. Thus all cell layers will show more or less the same temperature distribution. Considering that the x and y dimension of the entire LIBC are much bigger than the z dimension, temperature and current will likely show greater in plane gradients than cross plane gradients. Models of this scale also offer good insight into the cell behavior during adiabatic discharge. To simulate this thermal insulation is assumed at all boundaries.

4.5. Full 3D coupled

For higher discharge current or abuse conditions it is crucial to consider the entire cell geometry to get information of the cross plane distribution

as well. This full 3D model compromises 70 electrode sandwich layers. The current collectors, except for the top and bottom cathode are double coated. So, two electrode sandwiches always share their current collectors (see Table 1). Specific material characteristics are assigned to every single domain for the thermal and the electrochemical model. Only the heat transfer properties are averaged for the active material domains (anode, separator and cathode with electrolyte.)

This is certainly the most complex but also most informative model studied. It provides information that cannot be measured, like cross-plane temperature variation of the characteristics of the electrode sandwich at the center and local information for all dependent variables.

4.6. Thermal 3D

A purely thermal 3D model [6] is also examined. Its geometrical setup is identical to the fully coupled 3D model. The heat sources for every element are defined according to equations (2)-(4). This allows to clearly differentiate between reversible and irreversible heating and skips the complicated parametrization of the electrochemical model. However, there is a need to experimentally determine the internal resistance and the entropy in dependency of the cell temperature and depth of discharge.

5 Simulation Results

5.1. Model Verification

Figure 4 compares the simulated and measured cell voltage and the temperature development in the center of the top surface. Even though there are some deviations the fit is good enough to continue with the used set of parameters. The discrepancies towards the end of discharge are likely due to an increased internal cell resistance at this depth of discharge that is not considered in the simulation.

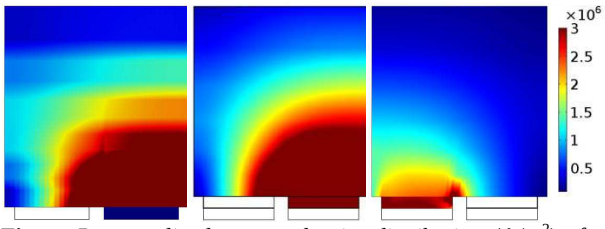

Figure 5: normalized current density distribution (A/m^2) after 1150s of 3C discharge: 1. Anode of adiabatic simulation of single layer model, 2.and 3.: full 3D model anode in cell center & top cathode

Both, the purely thermal and the fully coupled 3D model, show very good accordance with the experiment results for the overall surface temperature distribution and development displayed in Figure 3.

5.2. Current distribution

As expected, 3D simulations show huge gradients in the current density across the current collectors (Figure 5). This is hard to determine experimentally. For this cell format, however, it is not negligible. The variation in utilization in different parts of the current collectors and electrodes might lead to accelerated aging of cell parts that are exposed to the most stress. This can cause performance and safety issues.

When modelling LIBCs of this size, a uniform current distribution cannot be assumed. Depending on the desired output, 1D models and average coupling should thus be handled with care.

5.3. Temperature distribution

The temperature inside a battery is also difficult to measure in real life experiment. 3D simulations give a good overview of what the spatial distribution can look like. Figure 7 shows the difference between the in-plane temperature distribution in the center and at the surface of the cell. The maximal in-plane temperature gradient is about 4°C and similar for both locations. The center plane however is about 2°C to 3°C warmer than the surface plane. The difference is especially high close to the positive tab (see cross plane temperature distribution, Figure 6). This is also where the cell becomes the hottest during discharge, due to the constriction at the tabs and the smaller thermal conductivity of aluminium (positive current collector) compared to the negative copper current collector.

The purely thermal model delivers comparable results for the in cell temperature variation (see

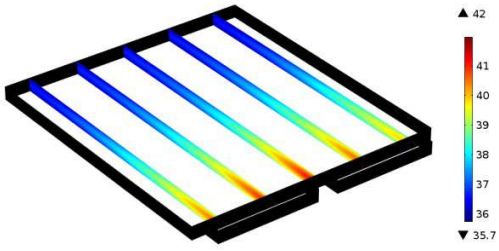

Figure 6: cross plane temperature distribution at the end of 3C discharge

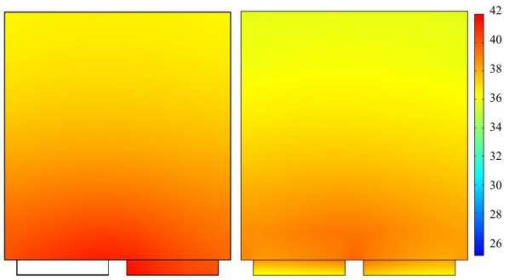

Figure 7: Comparison of the in-plane temperature distribution at the end of the 3C discharge, left: center of the cell, right: top surface

Figure 3), even though it assumes uniform current distribution (see Equation (4) and section 5.2). This is due to the precise experimental determination of the internal cell resistance and its dependence on the depth of discharge, which is not considered in the coupled model.

5.4. Computational costs

To investigate the cross-plane distribution, which is especially hard to attain experimentally, 2D models would be sufficient. However, they appear to be more numerically unstable and take longer to compute than the comparable 3D models. One explanation could be the big in-plane thickness for this format of LIBCs.

All simulations are run on a Dell Precision T7600 workstation with 128GB RAM and 2 E.10Ghz processors. Table 2 gives an overview about the computation time and required memory of the simulation of a 3C discharge without cooling plates. If the single layer model offers sufficient output information, e.g. to get an overview of the in-plane behavior, it is the preferred model, as it computes about 16 times faster than the other models. The thermal-only model on the other hand doesn't offer any computational advantages compared to the fully coupled model. It seems that the calculations of the heat source from the temperature and current dependent internal resistance create numerical difficulties. Especially at high temperatures, as the behavior of the internal resistance becomes highly nonlinear. Furthermore the mesh of the fully coupled 3D model with a total of 19593 elements is coarser than the mesh of the purely thermal model (322524 elements).

6 Conclusions

Multiphysics simulations like these offer good insight into the local current and temperature inside a LIBC. This information is hard to measure and can help to design safer and more reliable batteries without extensive expensive, time consuming and potentially risky experiments.

Especially, full 3D models, even though they require a higher computational effort, offer additional insight about the current distribution in the current collectors and electrodes and the cross plane temperature distribution.

7 References

1. M. Doyle, T.F. Fuller, J. Newman, Modeling of Galavanostatic Charge and Discharge of of the Lithium/Polymer/Insertion Cell, *J. Electrochem. Soc.*, **140**, 1526-1533 (1994)

2. J. Newman, K.E. Thomas-Alyea, *Electrochemical Systems*, 535ff. John Wiley & Sons Inc., Hoboken, New Jersey (2004)

	Solution time [s]	Physical memory [GB]	Virtual memory [GB]	Mesh elements	Model added value
1D Newman	85	1.1	1.24	48	+ fast validation electrochemical model
3D ES	1554	3.3	3.69	5448	+ in plane temperature and current distribution + sufficient for adiabatic conditions (coupled model validation) + 16x faster than full model
Full 3D	28097	70.44	75.94	195932	+ cross- and in- plane temperature and current distribution
Thermal 3D	28322	77.34	78	322524	- temperature only - assumes uniform current distribution + considers temperature dependency of internal resistance

Table 2: comparison of computation time, required memory, mesh size and model output

3. D. Bernardi, G. Pawlikowski, J.Newman; A General Energy Balance for Battery Systems*; J. Electrochem. Soc.*, **132**, 5-12 (1985)
4. P. J. Osswald, S. V. Erhard, J. Wilhelm, H. E. Hoster, and A. Jossen, Simulation and Measurement of Local Potentials of Modified Commercial Cylindrical Cells: I. Cell Preparation and Measurements, *J. Electrochem. Soc*. **162(10)**, A2099-A2105, (2015)
5. C. Wang V. Srinivasan, Computational battery dynamics (CBD)–electrochemical/ thermal coupled modeling and multi-scale modeling, *Journal of power sources*, **110**, no. 2, 364–376 (2002)
6. V. Srinivasan, C. Wang, Analysis of Electrochemical and Thermal Behavior of Li-Ion Cells, *J. Electrochem. Soc.*, **150**, (1) A98-A106 (2003)
7. G.-H. Kim, A. Pesaran, and R. Spotnitz, A three-dimensional thermal abuse model for lithium-ion cells, *Journal of Power Sources*, 170, no. 2, 476-489, (2007)
8. R. Arunachala, S. Arnold, L. Moraleja, T. Pixis, A. Jossen, J. Garche; 2015; Influence of Cell Size on Performance of Lithium Ion Battery; Oral presentation at Advanced Battery Power Conference Aachen (2015)
9. S. G. Stewart, V. Srinivasan, J. Newman, Modeling the Performance of Lithium-Ion Batteries and Capacitors during Hybrid-Electric-Vehicle Operation, *J. Electrochem. Soc.*, **155**, (9) A664-A671 (2008)
10. M. Ecker, S. Käbitz, I. Laresgoiti, D. U. Sauer, Parameterization of a Physico-Chemical Model of a Lithium-Ion Battery, *J. Electrochem. Soc.*, **162**, (9) A1849-A1857 (2015)
11. L. O. Valøen, J. N. Reimers, Transport Properties of LiPF6-Based Li-Ion Battery Electrolytes, *J. Electrochem. Soc.*, **152**, (5) A882-A891 (2005)
12. M. Safari, C. Delacourt, Modeling of a Commercial Graphite/LiFePO4 Cell, *J. Electrochem. Soc.*, **158,** (5) A562-A571 (2011)
13. S. Du, M. Jia, Y. Cheng, Y. Tang, H. Zhang, L. Ai, K. Zhang, Y. Lai, Study on the thermal behaviors of power lithium iron phosphate (LFP)aluminum-laminated battery with different tab configurations, *International Journal of Thermal Sciences*, **89,** 327-336 (2015)
14. A. Nyman, M. Behm, G. Lindbergh, Electrochemical characterisation and modelling of the mass transport, *Electrochimica Acta*, **53,** 356–6365 (2008)
15. T.G. Zavalis, M. Behm, G. Lindberg, Investigation of Short-Circuit Scenarios in a Lithium-Ion Battery Cell, *J. Electrochem. Soc.*, **159**, (6) A848-A859 (2012)

8 Acknowledgements

The presented work was supported by the Singapore National Research Foundation (NRF) through its Campus for Research Excellence and Technological Enterprise (CREATE) program.

9 Appendix

9.1. Model Parameters

Geometry

L_neg	0.000063	[m]	
L_sep	0.00002	[m]	
L_pos	0.00007	[m]	
L_neg_cc	0.0000075	[m]	
L_pos_cc	0.00001	[m]	
L_wid	0.243	[m]	
L_hei	0.222	[m]	
w_tab	0.09	[m]	
d_tab	0.015	[m]	
l_tab	0.012	[m]	
L_coat	0.000008	[m]	
Ncathode	36		

Electrochemical Model

rp_neg	1.10e-05	[m]	[9]
rp_pos	1.20e-06	[m]	[9]
epsl_pos	0.35	%	[9]
epsn_pos	0.32	%	[9]
epss_pos	0.33	%	[9]
epsl_neg	0.33	%	[9]
epsn_neg	0.168	%	[9]
epss_neg	0.502	%	[9]
epsl_sep	0.58	%	[10]
csmax_neg	46922	[mol/m^3]	calculated
csmax_pos	563537	[mol/m^3]	calculated
cs0_neg	0.85*csmax_neg	[mol/m^3]	fitted
cs0_pos	0.12*csmax_pos	[mol/m^3]	fitted
sigma_neg	100	[S/m]	[9]
sigma_pos	100	[S/m]	[9]
sigma_neg_cc	59900000	[S/m]	C*
sigma_pos_cc	37800000	[S/m]	C*
tplus	0.38		[11]
alpha_neg	0.489		[9]
alpha_pos	0.527		[9]
R_SEI	0.001		[12]
D_neg0	9.00E-14	[m^2/s]	[9]
D_pos0	5.00E-13	[m^2/s]	C*

kc0	2.00E-11	[m/s]	C*
ka0	2.00E-11	[m/s]	C*
Dl0(c)	8.794*10^(-11)*(c/1000)^2-3.972e-10*(c/1000)+4.862e-10		[14]
kl0(c)	0.1297*(c/1000)^3-2.51*(c/1000)^1.5+3.329*(c/1000)		[14]

Thermal Model

rhoAl	2700	[kg/m^3]	C*
rhocell	2086	[kg/m^3]	
rhoAc	1941	[kg/m^3]	calculated
rhoCo	8900	[kg/m^3]	C*
kAcxx	1.63	[W/(m*K)]	calculated
kAcyy	1.63	[W/(m*K)]	calculated
kAcyy	0.2	[W/(m*K)]	calculated
kcellxx	18	[W/(m*K)]	measurement
kcellyy	18	[W/(m*K)]	measurement
kcellyy	0.2	[W/(m*K)]	measurement
kAl	238	[W/(m*K)]	C*
kCo	400	[W/(m*K)]	C*
CpAl	900	[J/(kg*K)]	C*
CpCell	1305	[J/(kg*K)]	measurement
CpAc	1367	[J/(kg*K)]	C*
CpCo	385	[J/(kg*K)]	C*
rhocoat	1636	[kg/m^3]	[13]
Cpcoat	1377	[J/(kg*K)]	[13]
kcoat	0.427	[W/(m*K)]	[13]
EaDpos	35000	[J/mol]	[15]
EaDneg	30300	[J/mol]	[10]
EaDl	16500	[J/mol]	[11]
Eakc	43600	[J/mol]	[10]
Eaka	53400	[J/mol]	[10]
Eakl	4000	[J/mol]	[11]
dlnf/dlnc	(0.601-0.24*(0.001*c)^0.5+0.982*(1-0.0052*(T-298.15))*(0.001*c)^1.5)/(1-tplus)-1		[11]

*C: COMSOL Material Database or default value

9.2. List of symbols

α	Transfer coefficient
ε	Porosity, or volume fraction of electrolyte
η	Surface overpotential (V)
κ	Effective ionic conductivity (S/m)
σ_s	Effective electronic conductivity of porous electrode (S/m)
Φ	Eectrical potential (V)
c_l	Salt concentration in the electrolyte (mol/m^3)
c_s	Concentration of lithium in the solid insertion electrode (mol/m^3)
B	Bruggeman exponent
D_l	Salt diffusion coefficient of electrolyte (m^2/s)
$f_\pm$	Mean molar activity coefficient of the electrolyte
F	Faraday's constant, (96487C/mol)
i	Current density (A/m^2)
i_n	Transfer current normal to the surface of the active material (A/m^2)
i_0	Exchange current density (A/m^2)
I	Total current density in the cell (A/m^2)
j_n	Molar flux due to reaction ($mol/s \cdot m^2$)
k_a, k_c	Rate constants for the anodic and cathodic directions of a reaction
n	Number of electrons transferred in electrode reaction
r	Radial position across a spherical particle (m)
R	Universal gas constant, (8.3143 $J/mol \cdot K$)
R_s	Radius of solid particles (m)
s	Stoichiometric coefficient, positive for anodic reactants
t_i^0	Transference number of species i with respect to the solvent
U	Open-circuit potential (V)
z	Change of reacted species
ρ	Density (kg/m^3)
c_p	Heat capacity (J/kg K)
T	Temperature (K)
t	Time (s)
k	Heat conductivty (W/m K)
Q	Heat generation (W/m^3)
$R_{internal}$	Internal resitance (Ω)
ΔS	Change in entropy